Centreline and cross-glacier air temperature variability on an Alpine glacier: assessing temperature distribution methods and their influence on melt model calculations

THOMAS E. SHAW,[1,2] BEN W. BROCK,[1] ÁLVARO AYALA,[3] NICK RUTTER,[1] FRANCESCA PELLICCIOTTI[1]

[1]*Department of Geography, Northumbria University, Newcastle, UK*
[2]*Advanced Mining Technology Center, Universidad de Chile, Santiago, Chile*
[3]*Laboratory of Hydraulics, Hydrology and Glaciology (VAW) ETH Zurich, Zurich, Switzerland*
Correspondence: Thomas E. Shaw <thomas.shaw@amtc.uchile.cl>

ABSTRACT. The spatio-temporal distribution of air temperature over mountain glaciers can demonstrate complex patterns, yet it is often represented simplistically using linear vertical temperature gradients (VTGs) extrapolated from off-glacier locations. We analyse a network of centreline and lateral air temperature observations at Tsanteleina Glacier, Italy, during summer 2015. On average, VTGs are steep ($<-0.0065\,°C\,m^{-1}$), but they are shallow under warm ambient conditions when the correlation between air temperature and elevation becomes weaker. Published along-flowline temperature distribution methods explain centreline observations well, including warming on the lower glacier tongue, but cannot estimate lateral temperature variability. Application of temperature distribution methods improves simulation of melt rates (RMSE) in an energy-balance model by up to 36% compared to the environmental lapse rate extrapolated from an off-glacier station. However, results suggest that model parameters are not easily transferable to glaciers with a small fetch without recalibration. Such methods have potential to improve estimates of temperature across a glacier, but their parameter transferability should be further linked to the glacier and atmospheric characteristics. Furthermore, 'cold spots', which can be $>2°C$ cooler than expected for their elevation, whose occurrence is not predicted by the temperature distribution models, are identified at one-quarter of the measurement sites.

KEYWORDS: energy balance, glacier mass balance, glacier meteorology, glacier modelling

1. INTRODUCTION

Near-surface air temperature (T_a) is a crucial component of the glacier surface energy balance (Ohata, 1992; Hock, 1999; Ohmura, 2001) and a fundamental control on the melt rate at a snow or ice surface (Petersen and Pellicciotti, 2011). As such, accurate quantification of T_a in distributed melt models is required for studies of glacier mass balance (e.g. Reijmer and Hock, 2008; Engelhardt and others, 2013, Gabbi and others, 2014), water resource availability (e.g. Nolin and others, 2010) and glacier contributions to sea-level rise (e.g. Hock and others, 2009). Recent work has investigated T_a variability and sought to improve understanding of its physical controls in space and time, both with respect to debris-free (Shea and Moore, 2010; Petersen and Pellicciotti, 2011; Petersen and others, 2013; Ayala and others, 2015; Carturan and others, 2015) and debris-covered glaciers (Shaw and others, 2016; Steiner and Pellicciotti, 2016). However, in the absence of local data, or due to modelling constraints, a constant and uniform linear 'lapse rate' such as the environmental lapse rate (ELR = $-0.0065\,°C\,m^{-1}$) is commonly applied when distributing air temperature across entire glaciers (e.g. Arnold and others, 2006; Nolin and others, 2010).

Published 'lapse rates' (referred to hereafter as vertical temperature gradients or 'VTGs') on glaciers vary significantly across the literature and are determined by both surface and atmospheric conditions (Marshall and others, 2007). Several studies have demonstrated that, over melting ice surfaces,

VTGs tend to be shallow or absent due to the development of a katabatic boundary layer (KBL) under warm ambient conditions (Greuell and Böhm, 1998; Shea and Moore, 2010; Petersen and others, 2013; Ayala and others, 2015) which often result in thermal inversions (Strasser and others, 2004; Carenzo, 2012). However, evidence of erosion into the KBL by warm up-valley winds and/or synoptically forced flow has been shown to lead to more negative VTGs and a stronger dependency on elevation (Pellicciotti and others, 2008; Petersen and Pellicciotti, 2011).

Carturan and others (2015) observed average VTGs that are more negative than the ELR on three small alpine glaciers in the Ortles-Cevedale range, Italy. This was explained by the weak effect of the KBL in modifying free-air temperatures on these small fragmenting glaciers. Other studies have reported similar findings that average VTGs can be steep ($<-0.0065\,°C\,m^{-1}$) over melting glaciers (Konya and others, 2007; Anslow and others, 2008; MacDougall and Flowers, 2011; Ragettli and Pellicciotti, 2012). However, in general, constant linear gradients of T_a have been shown to account poorly for much of the diurnal variability in on-glacier observations (Petersen and Pellicciotti, 2011), particularly when extrapolated from off-glacier sites outside of the glacier boundary layer.

Accordingly, attempts have been made to account for the presence of the KBL over melting glaciers using physically orientated (Greuell and Böhm, 1998; Petersen and others, 2013; Ayala and others, 2015; Carturan and others, 2015)

and statistical approaches (Shea and Moore, 2010; Carturan and others, 2015). Such approaches have been successful in replicating the observed cooling and dampening effect of the KBL on the diurnal temperature signal (Carturan and others, 2015), though still face some uncertainty in how generalis-able they are and how well they account for T_a away from the glacier centreline (Hannah and others, 2000; Shea and Moore, 2010). Findings for the Swiss Haut Glacier d'Arolla (hereafter 'Arolla') have further demonstrated the complexity of the spatial variability in on-glacier T_a. Ayala and others (2015) identified a cooling of down-glacier air temperature alongside relatively warm temperatures on the glacier tongue. This latter effect has been considered to be due to the entrainment of warm air in upper layers of the glacier surface boundary layer, advection of heat from surrounding topography, the warming effect of debris cover or turbulent mixing (van den Broeke, 1997; Greuell and Böhm, 1998; Munro, 2006; Shea and Moore, 2010; Reid and others, 2012).

Few studies have the quantity of observations necessary to explore T_a variability and test recently proposed models, and fewer still have investigated lateral variations and their causes (e.g. van de Wal and others, 1992; Hannah and others, 2000; Strasser and others, 2004; Shea and Moore, 2010). To address these limitations, the aims of this study are to (1) analyse a new dataset of centreline and lateral tem-perature observations over an alpine glacier during the summer ablation season, (2) assess the applicability of pub-lished parameterisations which account for along-glacier air temperature variations and (3) evaluate their ability to represent measured melt rates using a physically based melt model.

2. STUDY SITE

Soches-Tsanteleina Glacier (hereafter referred to as Tsanteleina Glacier) is a relatively small debris-free glacier within the Grand Sassiere-Rutor mountain group, located near to the Gran Paradiso National Park at the head of the Val di Rhêmes, Italy (45°28′51″N 7°03′41″E). The north-northeast facing valley glacier (see Fig. 1) has an area of ~2.65 km^2 and an elevation range of 2800–3445 m a.s.l. The north side of the glacier is constrained by the 3250 m a.s.l. high Granta Parei, and the Punta Tsanteleina to the west (3600 m a.s.l.), respectively, shading the lower tongue and the upper glacier in the evening. The glacier slope ranges between 3° and 29° and averages ~11°. The gentle surface slope steepens at ~3100 m a.s.l. below a plateau at ~3200 m a.s.l. before another steep rise to the upper accu-mulation area.

3. DATA

3.1. Temperature and meteorological measurements

Measurements of T_a were made at 14 on-glacier sites using Gemini TinyTag thermistors housed 2 m from the surface in naturally ventilated Campbell MET20/MET21 radiation
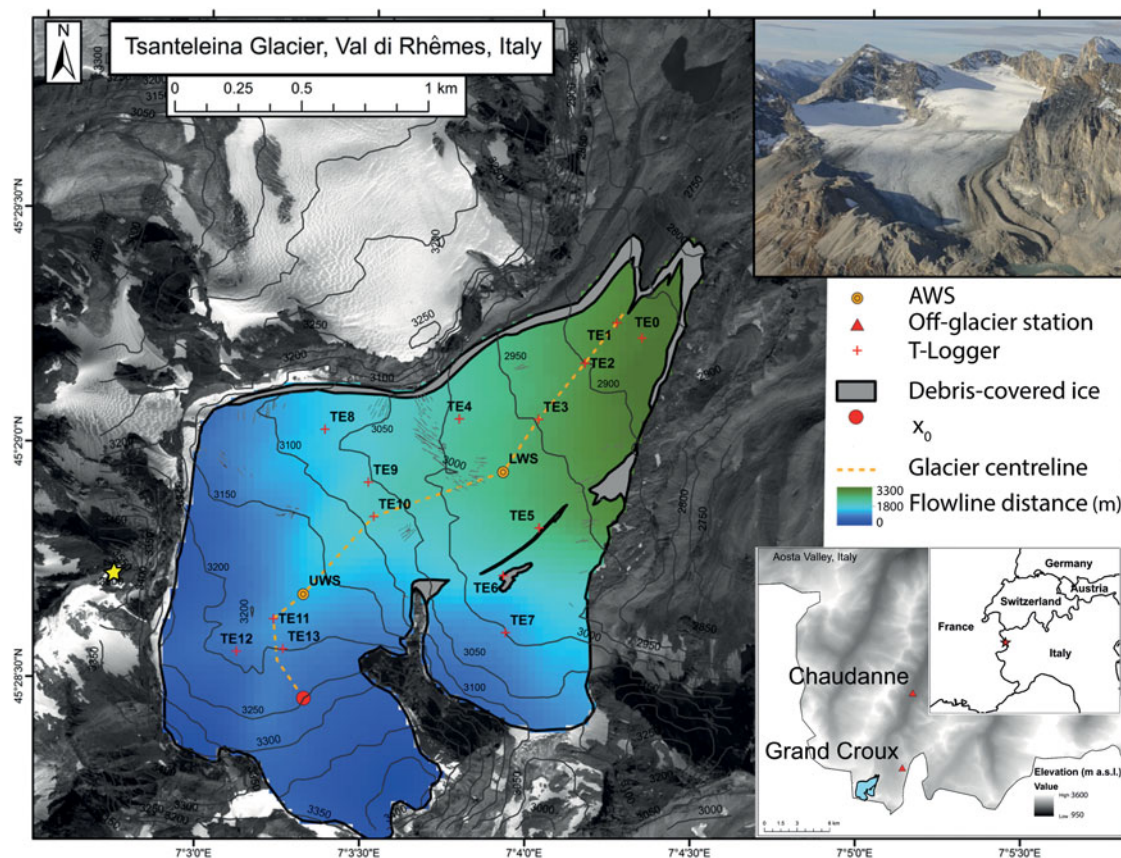

Fig. 1. Map of Tsanteleina Glacier with the location of the T-loggers (indicated by 'TE') and automatic Weather Stations, LWS and UWS. The location of the off-glacier stations Chaudanne and Grand Croux is shown in the Aosta Valley map insert (bottom right). Distance along the flowline is indicated by the colour scale calculated using SAGA GIS. The location of x_0 is shown by the red dot. The centreline stations are indicated by the orange line. The yellow star indicates the location of Punta Tsanteleina. Background satellite imagery courtesy of a DigitalGlobe Foundation imagery grant. Upper right insert shows an aerial image looking up-glacier (source: Fondazione Montagna Sicura).

shields on free-standing tripods (hereafter referred to as T-loggers and indicated by TE(*n*) – see Fig. 1, with details in Table 1). TinyTag sensors are either TGP-4520 loggers with a PB 5001 probe type (accuracy ±0.20°C) or TG-4505 loggers with temperature-relative humidity sensors (accuracy ±0.35°C – see Table 1). The distribution of stations was designed to sample the variability of T_a along the centreline of the glacier (determined as a maximum horizontal distance from the lateral glacier boundary) and at lateral positions to the side of a lower weather station (LWS) and of T-Logger TE10 (Fig. 1). Sites TE11–13 and an upper weather station (UWS) are located in the 2015 glacier accumulation zone (Fig. 1). TE10 is sited below a steeper slope (20°) at the approximate equilibrium line altitude of ~3100 m a.s.l. The T-loggers on the glacier tongue (TE0 and TE1) are at similar elevations and are ~100 m apart. The location of TE1 is considered to better represent the centreline of the glacier, based on the distance to the lateral glacier margins.

Off-glacier T_a data were available from two locations near to Tsanteleina Glacier: Grand Croux (GC), 2 km northeast from the glacier tongue at a similar elevation to the glacier tongue (2750 m a.s.l.) and a valley site Chaudanne (CH), ~8.5 km north from the tongue (1794 m a.s.l. – see Fig. 1). Data from GC and CH were provided by the Regione Autonoma Valle d'Aosta, including precipitation data at CH (Table 1).

On-glacier meteorological and energy-balance data were collected at lower and upper automatic weather stations, LWS (2986 m a.s.l., ablation zone) and UWS (3145 m a.s.l., accumulation zone), respectively, which sampled data every 5 s and recorded at 30 min intervals on Campbell CR3000 data loggers. All AWS and T-logger data were processed into hourly means for analysis. The meteorological data available consists of T_a and relative humidity (TinyTag TGP-4520 for LWS and Campbell HMP45C for UWS –

accuracy also ±0.2°C), incoming and outgoing shortwave and longwave radiation (Kipp and Zonen CNR4 for LWS) and wind speed/direction (Campbell open path eddy covariance sonic anemometer and Young 05103 anemometer for LWS and UWS, respectively). All variables were measured at ~2 m height.

Stations were installed on the glacier on 19 June and removed on 14 September. Because several T-logger stations fell over due to differential ablation, the available data for analysis of T_a variability was split into two periods, 17 July–2 August ('Jul–Aug' hereafter) and 16 August–14 September ('Aug–Sep' hereafter). For the two periods of 'best data' availability (Fig. 2), small (<30 h) data gaps still exist for some stations (indicated in Table 1). Stations with data gaps were excluded from the calculation of regression-derived VTGs for that time step and temperature distribution models (see Methodology section) were not calculated for time steps where data gaps existed. Larger data gaps at TE11–13 exist for the Aug–Sep period (~70% of this period).

Intercomparison tests of all T-loggers at off-glacier locations were performed to understand the reliability of our on-glacier data and provide suitable thresholds indicating significant temperature differences between sites, independent of manufacturer or measurement errors. The intercomparison tests revealed instantaneous temperature differences between individual sensors and the mean temperature of all remaining sensors to be ≤0.30°C (maximum SD of any individual sensor = 0.14°C) using a leave-one-out analysis. Tests revealed no bias in T-logger differences under high insolation and low wind speed conditions (Georges and Kaser, 2002). The details of these tests are given in the Supplementary Information. Based on these results, we interpret differences between individual sensors of >0.30°C as indicative of real temperature differences at different locations on Tsanteleina Glacier.

Table 1. Station details including coordinates, elevation and measured variables

Station	Northing	Easting	Elevation (m a.s.l.)	Variables	Jul–Aug	Aug–Sep
TE0[a,r]	5 039 031	349 383	2885	T_a, RH	O	
TE1[a,t]	**5 039 077**	**349 331**	**2879**	**T_a**	**O**	**O**
TE2[b,t]	**5 038 918**	**349 206**	**2902**	**T_a**		
TE3[b,r]	**5 038 697**	**349 023**	**2947**	**T_a, RH**	**O**	
TE4[b,t]	5 038 699	348 710	2987	T_a		
TE5[a,r]	5 038 271	349 024	2977	T_a, RH		O
TE6[b,t]	5 038 083	348 882	3003	T_a		
TE7[b,t]	5 037 858	348 891	3014	T_a	X	
TE8[a,t]	5 038 658	348 181	3089	T_a		
TE9[a,t]	5 038 451	348 351	3072	T_a	O	
TE10[a,t]	**5 038 316**	**348 372**	**3088**	**T_a**		
TE11[b,t]	**5 037 913**	**347 977**	**3197**	**T_a**		**X**
TE12[a,r]	5 037 784	347 831	3199	T_a, RH		X
TE13[a,t]	**5 037 794**	**348 014**	**3208**	**T_a**		**X**
LWS[b,t]	**5 038 491**	**348 883**	**2986**	**T_a, u, v, Rad$_{NET}$, RH**		
UWS[b]	**5 038 009**	**348 094**	**3145**	**T_a, u, v, Rad$_{NET}$, RH**		
GC	5 040 056	352 791	2750	T_a		
CH	5 046 941	351 824	1794	T_a, Precip		

The last columns indicate the availability of data for the 2015 ablation season in July–August (Jul–Aug) and August–September (Aug–Sep) where an 'O' indicates minor data gaps and an 'X' indicates larger gaps in the data for the period. Northing and easting values are reported in UTM 32N. Centreline stations are shown in bold text. 'T_a', air temperature; 'u', wind speed; 'v', wind direction; 'Rad$_{NET}$', all fluxes of net radiation; 'RH', relative humidity.
a, MET20 radiation shield;.
b, MET21 radiation shield;.
t, temperature TinyTag (accuracy ±0.20°C);.
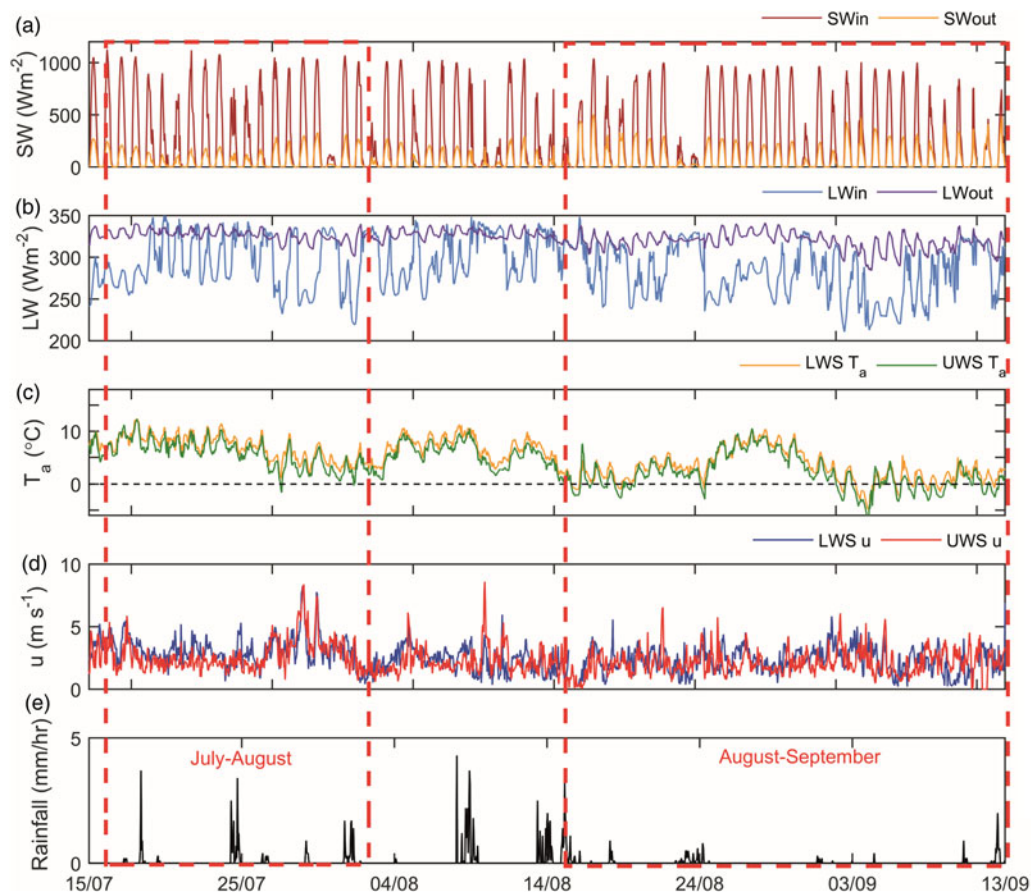r, temperature/relative humidity TinyTag (accuracy ±0.35°C).

Fig. 2. Tsanteleina Glacier meteorological conditions for the entire data period of 2015 including the two outlined periods of 'best T-logger data availability': (a) incoming and reflected shortwave radiation (W m^{-2}) at LWS, (b) incoming and outgoing longwave radiation (W m^{-2}) at LWS, (c) T_a at both AWSs (°C), (d) wind speed (m s^{-1}) measured at both AWSs and (e) the precipitation rate (mm hr^{-1}) recorded at Chaudanne station.

3.2. Mass-balance measurements

Surface lowering was measured (for the dates of each period) using 3 m PVC stakes installed at each station site below UWS (Fig. 1), using a Kovacs ice drill. The measurements were converted to w.e. values using an average snow density of 565 kg m^{-3}, calculated from a 1.08 m snow pit at TE11 (dug 16 July), and an assumed ice density of 900 kg m^{-3}. Due to logistical constraints in the field, no measurements of mass balance were possible at elevations above TE10.

3.3. Additional data

Elevation information for the glacier was provided by a 30 m resolution ASTER (Advanced Spaceborne Thermal Emission and Reflection Radiometer) global digital elevation model (DEM), with an estimated elevation error of ±1 m (Tachikawa and others, 2011). Boundaries of the glacier were determined using a high-resolution Digital Globe image for the valley, taken on 30 September 2014 (Courtesy of Digital Globe Foundation).

4. METHODOLOGY

4.1. Distributing temperature with VTGs

A reference centreline VTG (hereafter 'VTG$_{CL}$') was calculated from regression of all centreline stations with elevation (orange line in Fig. 1, stations in bold type in Table 1). This enabled the difference in T_a at lateral stations relative to the expected centreline temperature at the same elevation to be calculated. An off-glacier VTG was calculated between the permanent CH and GC stations (see Data section) for each time step and the ELR was used to extrapolate air temperature from both off-glacier locations. The summary of temperature distribution methods used in this study and their acronyms are given in Table 2.

4.2. Variability of on-glacier VTGs under different conditions

Following the approach of Shaw and others (2016), we investigate the steepness and elevation dependency of on-glacier VTGs separately for day and night hours (day is classified as 07:00–20:00 inclusive) and different meteorological conditions. This sub-setting of meteorological conditions was based on: (1) cloud cover fraction parameterised as a function of longwave radiation (following Juszak and Pellicciotti, 2013), (2) different wind speed percentiles (upper and lower 10%) and (3) off-glacier air temperature percentiles (upper and lower 10%, following Ayala and others, 2015). We note that T_a at all on-glacier stations is compared with these subsets for identical time steps in order to observe the structure of on-glacier T_a and the applicability of a linear VTG.

Table 2. Methods of air temperature distribution with acronyms used in the text

Acronym	Description	Value range Jul–Aug	Value range Aug–Sep
VTG_{CL}	An on-glacier VTG derived from regression of elevation and T_a at each centreline station (Fig. 1, Table 1) for each hourly time step.	−0.0177/+0.0033 (−0.0075)	−0.0179/+0.0239 (−0.0068)
GC_{ELR}	The constant environmental 'lapse rate' extrapolated from high-altitude, off-glacier station Grand-Croux.	−0.0065	−0.0065
GC_{off}	A locally derived (Chaudanne–Grand Croux) VTG extrapolated from high-altitude, off-glacier station Grand Croux.	−0.0121/+0.0031 (−0.0050)	−0.0119/+0.0022 (−0.0046)
CH_{ELR}	The constant environmental 'lapse rate' extrapolated from valley, off-glacier station Chaudanne.	−0.0065	−0.0065
$SM_{10}/$ SM_{opt}	Shea and Moore (2010) statistical parameterisation applied to extrapolated GC_{ELR} temperatures over the glacier.	–	–
ModGB	Modified thermodynamic model (Ayala and others, 2015) initiated with 'top of flowline' (x_0) temperature (T_0) derived from GC_{ELR}.	–	–

VTG ranges and means (in parentheses) are given for the Jul–Aug and Aug–Sep periods. A positive VTG indicates that temperature increases with increasing elevation.

4.3. Temperature distribution models

The approaches of Shea and Moore (2010) and Ayala and others (2015) were applied to reproduce measured T_a variability on Tsanteleina Glacier as a function of flowline distances (the average distance from an upslope summit or ridge – Fig. 1) using off-glacier T_a data alone. We refer to these methods as SM and ModGB, respectively. We utilise the up-valley off-glacier site, GC (2750 m a.s.l.) as the main source of off-glacier air temperature, as it is not affected by a glacier cooling effect or daytime shading.

The SM approach estimates T_a using a statistical model to account for the observed differences in measured and extrapolated ambient temperature (T_{amb}), considered as the air temperature outside the thermal influence of the glacier. This method follows the form:

$$T_a = \begin{cases} T_1 + k_2(T_{amb} - T^*), T_{amb} \geq T^* \\ T_1 - k_1(T^* - T_{amb}), T_{amb} < T^* \end{cases}, \quad (1)$$

where T_{amb} is distributed using GC_{ELR} (Table 2), T^* (°C) represents the threshold ambient temperature for katabatic flow and T_1 is the corresponding threshold near-surface temperature over the glacier. Parameters k_1 and k_2 are the sensitivities of near-surface temperature to ambient temperature below and above the threshold T^* (Shea and Moore, 2010). Following the methodology of Carturan and others (2015), T^* was calculated as a function of distance along the flowline (DF):

$$T^* = \frac{C_1 DF}{C_2 + DF}, \quad (2)$$

where C_1 (6.61) and C_2 (436.04) are fitted coefficients reported in Carturan and others (2015). Slopes of the linear piecewise regressions (k_1 and k_2) were modelled as exponential functions of the DF according to the original study:

$$k_1 = \beta_1 \exp(\beta_2 DF), \quad (3)$$

$$k_2 = \beta_3 + \beta_4 \exp(\beta_5 DF), \quad (4)$$

where β_i are the fitted coefficients. The corresponding on-glacier temperature T_1 was calculated as $T^* \cdot k_1$ (Shea and Moore, 2010). The original fitted parameters were found to model T_a well across La Mare Glacier in the Ortles-Cevedale range, Italy (Carturan and others, 2015). Here we apply the

original parameters of Shea and Moore (2010), referred to as SM_{10}, and the parameters (k_1 and k_2) fitted to the data for centreline stations on Tsanteleina Glacier, referred to as SM_{opt}.

The modified form of the thermodynamic model (Greuell and Böhm, 1998), referred to as ModGB, follows the form:

$$T_a(x) = (T_0 - T_{eq}) \exp\left(\frac{-x - x_0}{L}\right) + T_{eq} + K\left(\frac{x - x_0}{L}\right), \quad (5)$$

where T_0 (°C) is the air temperature at the theoretical location where air enters the KBL x_0 (selected by visual inspection of the mid accumulation area following Ayala and others, 2015). T_0 is also derived from extrapolated T_a using the GC_{ELR} method (Table 2). T_{eq} is the 'equilibrium temperature' and L (metres) is the length scale. The original form of the model (Greuell and Böhm, 1998) attempts to explain down-glacier cooling within the KBL, while last term was introduced by Ayala and others (2015) to account for observed warming on glacier tongues with an empirical factor K (°C). L is calculated according to the original study of Greuell and Böhm (1998) by:

$$L = \frac{H \cos(a)}{B_H}, \quad (6)$$

where H is the height of the boundary layer (m), B_H represents the bulk transfer coefficient for heat and a is the mean glacier slope (°). T_{eq} is derived from:

$$T_{eq} = bL, \quad (7)$$

where b is calculated using the dry adiabatic lapse rate Γ_d by:

$$b = \Gamma_d \tan(a), \quad (8)$$

Following Ayala and others (2015), H and K are used as tuning parameters when fitting the model to observations of T_a along the glacier centreline during warm ambient conditions. The derivation of the original thermodynamic model is explained in detail in Greuell and Böhm (1998) and not repeated here. Ayala and others (2015) suggest that the original model (of Greuell and Böhm, 1998) is not applicable to small glaciers with a short fetch. As such, the original model form is not included in the analysis of Tsanteleina Glacier. SM and ModGB parameters for Tsanteleina Glacier are derived from all available data for the combined Jul–Aug and Aug–Sep

periods and used to distribute temperature in the separate periods for melt modelling (see Melt modelling section).

As an input to an energy-balance model, ModGB is applied only for T_0 temperatures $\geq 6°C$, where parameters begin to converge for previously studied glaciers (Ayala and others, 2015, 2017). These studies have shown that on-glacier temperatures are well reproduced by linear gradients below this T_0 threshold, and we thus apply GC_{ELR} (Table 2) for $T_0 < 6°C$.

4.4. Melt modelling

The importance of different methods of air temperature distribution to melt model calculations is assessed through their application in a physically based energy-balance model (Reid and others, 2012) applied at distributed stake locations on Tsanteleina Glacier. Melt (M) is calculated for the given time step (Δt) by:

$$M = \frac{Q_m \Delta t}{p_w L_f}, \tag{9}$$

where L_f is latent heat of fusion (J kg^{-1}), p_w is the density of water (kg m^{-3}) and Q_m is the energy available for melt, calculated as:

$$Q_m = S_{net} + L_{net} + H + L_E + P + G, \tag{10}$$

where S_{net} and L_{net} are the net fluxes of shortwave and longwave radiation, respectively, H and L_E are the turbulent fluxes of sensible and latent heat, P is the heat flux provided by rain and G is the conductive heat flux into the snow or ice. Model calculations were performed on a 30 m gridcell size, consistent with the available ASTER GDEM resolution.

Wind speed and relative humidity were treated as spatially constant values from the LWS (UWS) below (above) 3100 m a.s.l. in order to treat the upper and lower glaciers with the most locally available data. Summer snow accumulation was estimated at each site using precipitation data at CH (Fig. 1), a precipitation gradient of 0.0026 mm h^{-1} m^{-1} (Fyffe and others, 2014) and a liquid precipitation threshold of 1°C (Jóhannesson and others, 1995; MacDougall and others, 2011). Snow accumulation was negligible during Jul–Aug, but contributed a total of 0.28 m w.e. to the LWS site during Aug–Sep (Fig. 2e).

Binary grids were created utilising the hill shade algorithm in ArcGIS (Shaw and others, 2016) to identify shaded glacier cells at each time step. The proportions of direct and diffuse radiation recorded at LWS were calculated and distributed across glacier accounting for cell slope and aspect using the equations in Brock and Arnold (2000) and a sun position algorithm (Reda and Andreas, 2008). Surface roughness (z_0) was calculated at 14 locations across the whole glacier in July 2015 using the microtopographic method (Munro, 1989; Brock and others, 2006) and interpolated using inverse distance weighting. The obtained values lie within the range of the literature (see Brock and others, 2006) and vary from 2 mm (smooth ice) to 16 mm (crevasse fields).

4.5. Evaluation of temperature distribution models

Model performance and the effectiveness of the different temperature distribution methods are evaluated by comparing measured melt rates at centreline and lateral sites

(which have stake data in both periods) to modelled melt from the different T_a distribution methods outlined in Table 2. Modelled melt rates are also compared to a reference model using measured air temperature and assessed with respect to the potential manufacturer errors in the temperature input data. T_a values are varied $\pm 0.35°C$ (the maximum error range for the TinyTag loggers) uniformly across all input data prior to the reference model run and compared to the melt estimation from the different temperature distribution methods.

5. RESULTS: OBSERVED TEMPERATURE VARIABILITY

5.1. Temperature variability under different meteorological conditions

Mean station T_a values conform to an approximate linear relationship with elevation, particularly when only considering the centreline stations (Fig. 3). Table 3 shows the mean VTGs for all subsets of time and meteorological conditions. Mean VTGs for all subsets are similar to, or more negative than the ELR, with the exception of high off-glacier temperatures (90th percentile, see Methodology section). This is particularly the case during Aug–Sep, when the on-glacier temperature distribution can no longer be explained by elevation (low, non-significant R^2 values in Table 3). In contrast, under the coldest off-glacier temperatures (tenth percentile, typically clear nights), VTGs become very steep and a strong relationship to elevation is evident.

Generally, night-time VTGs are steeper than daytime, particularly in Jul–Aug; although day/night differences are less distinct in general than between high- and low-temperature conditions (Table 3). Overcast conditions had little effect
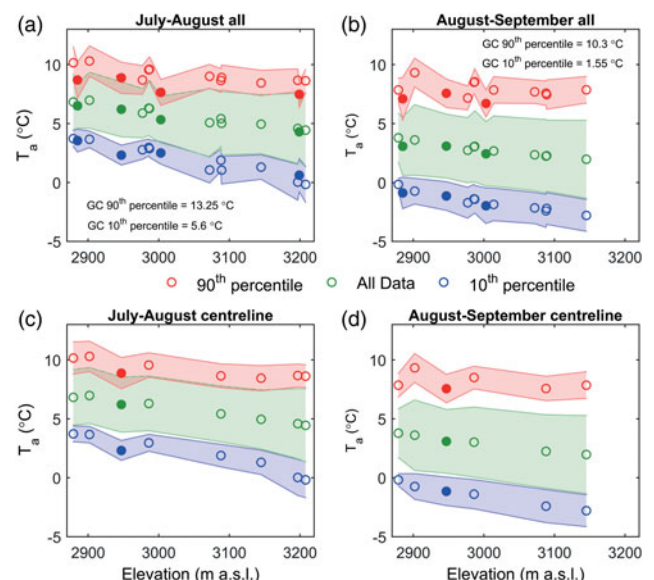

Fig. 3. Mean T_a-elevation relationships for all stations (upper panels) and centreline stations only (lower panels). The circles indicate mean T_a (green), and the means of the 90th (red) and tenth (blue) percentiles of off-glacier temperatures at Grand Croux (GC) station. The shaded area represents one SD (this is larger for the green plots as they represent all data). Data for TE11–13 are not shown for Aug–Sep due to larger data gaps. Sites investigated as cold spots (Fig. 4) are shown by the filled circles. Their elevation information is given in Table 1.

Table 3. Vertical temperature gradients (VTG) derived from linear regression of temperature observations against elevation for all available on-glacier data in each period and for different conditions

Condition	n	July–August (408)		n	August–September (720)	
		All stations	Centreline		All stations	Centreline
All data	408	−0.0073 (0.90[a])	−0.0075 (0.97[a])	720	−0.0060 (0.83[a])	−0.0068 (0.97[a])
High off-glacier T_a	41	−0.0040 (0.29[b])	−0.0047 (0.66[a])	72	−0.0014 (0.05[x])	−0.0026 (0.04[x])
Low off-glacier T_a	41	−0.0109 (0.91[a])	−0.0109 (0.91[a])	72	−0.0085 (0.91[a])	−0.0094 (0.97[a])
Day	204	−0.0063 (0.88[a])	−0.0064 (0.96[a])	360	−0.0059 (0.82[a])	−0.0066 (0.98[a])
Night	204	−0.0088 (0.92[a])	−0.0090 (0.97[a])	360	−0.0063 (0.84[a])	−0.0071 (0.97[a])
Clear sky	46	−0.0079 (0.87[a])	−0.0074 (0.88[a])	91	−0.0080 (0.58[a])	−0.0094 (0.72[b])
Overcast	138	−0.0075 (0.96[a])	−0.0074 (0.97[a])	206	−0.0048 (0.92[a])	−0.0052 (0.98[a])
High wind speeds	41	−0.0074 (0.93[a])	−0.0071 (0.96[a])	72	−0.0071 (0.78[a])	−0.0081 (0.87[a])
Low wind speeds	41	−0.0074 (0.78[a])	−0.0078 (0.95[a])	72	−0.0047 (0.76[a])	−0.0056 (0.98[a])

VTGs are reported in °C m^{-1} with R^2 (coefficient of determination) values in parentheses for means of all stations (including lateral stations) and centreline stations only
[a]Indicates where the R^2 relationship is statistically significant to the 99% level, [b]where it is significant at the 95% level and [x]where it is not statistically significant.

on VTG magnitude compared with clear sky conditions in Jul–Aug, but were associated with much less negative VTGs in Aug–Sep. Elevation dependency of T_a is strong (high R^2 values) for overcast conditions in both periods.

5.2. Lateral and centreline anomalies

As shown in Table 3, elevation becomes a poorer predictor of T_a when lateral stations are included, evident from the reduction in R^2 (coefficient of determination) for all stations in both periods. Furthermore, for the warmest conditions, cross-glacier T_a variability is greatest (Figs 3a, b).

Lateral sites TE0, TE6 and TE12 (Fig. 1) frequently exhibited lower T_a than expected when compared with centreline temperatures for the same elevations (Fig. 3). Furthermore,

centreline site TE3 also exhibited notably cooler temperatures during both periods than its elevation would suggest (these stations are indicated by filled circles in Fig. 3). Hourly temperature deviations at these sites were quantified by comparison with the centreline temperatures estimated for their elevations, based on VTG$_{CL}$ (Table 2).

Hourly T_a depressions at these sites are largest at relatively low, but not calm, wind speeds of 2–3 m s^{-1} (derived from the nearest weather station) under warm, high-pressure conditions (Fig. 4). During periods of low-pressure and high synoptically forced wind speeds, differences from the centreline T_a are very small, particularly for TE0 and TE6. This feature is less consistent for sites TE3 and TE12, which also show several hours of positive temperature anomaly for moderately high pressure and low-to-moderate wind speeds. The lowest 10% of wind speed values (≤1 m s^{-1}) resulted in less negative (though significant) VTGs in Aug–Sep, though wind speed percentiles show no clear differences in elevation dependency or slope of VTGs for Jul–Aug (Table 3).
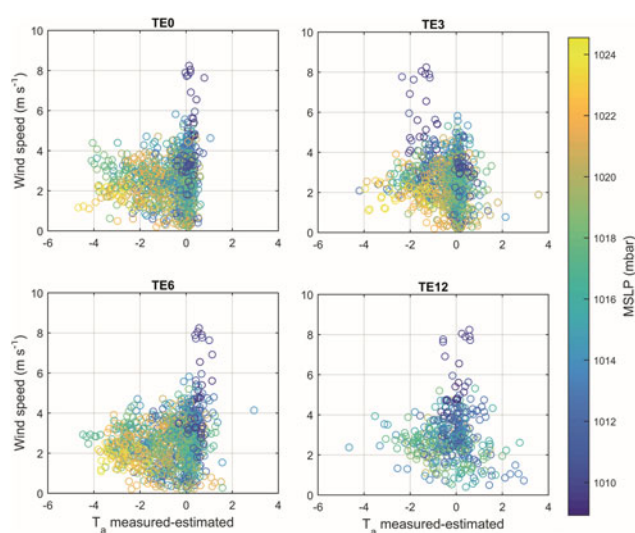

Fig. 4. The difference in measured T_a at three lateral sites (TE0, TE6 and TE12) and one centreline site (TE3) from T_a estimated by VTG$_{CL}$ (x-axis), plotted against wind speed at LWS (UWS for TE12) (y-axis) and mean sea-level pressure (colour scale) derived from the ERA-interim reanalysis dataset (http://apps.ecmwf.int/datasets/data/interim-full-daily/levtype=sfc/). Reanalysis data were linearly interpolated from 6-hourly to hourly intervals to correspond with hourly data for Tsanteleina. Negative x-axis values indicate that station temperatures are cooler than the corresponding elevation on the centreline.
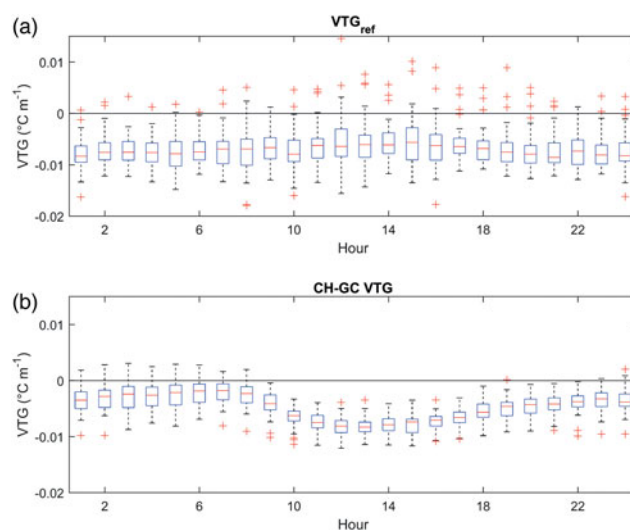

Fig. 5. Boxplots of hourly VTGs for (a) centreline stations (VTG$_{CL}$) and (b) between off-glacier stations Chaudanne (1794 m a.s.l.) and Grand Groux (2750 m a.s.l.) in both periods. Boxplot limits show the 25th and 75th percentiles and outliers are shown by the red crosses.

6. RESULTS: TEMPERATURE ESTIMATION

6.1. Off-glacier VTGs

The VTG between the two off-glacier stations CH and GC fluctuates between strong negative ($<-0.0100\ °\mathrm{C\ m}^{-1}$) gradients to moderate inversions (up to $+0.0031\ °\mathrm{C\ m}^{-1}$) over their large elevation difference (>900 m – Fig. 5). Due to the position of the CH in Val di Rhêmes, cold air which sinks into the valley during the night results in a frequent inversion layer whereby the GC station is warmer. This reiterates the suggestions of Oerlemans (2001) and Carturan and others (2015) that high-altitude stations are preferable to those within valleys for distributing air temperature.

The mean diurnal variation of the off-glacier VTG is generally the inverse of that of the glacier centreline, though with less variance (Fig. 5). During the day, VTGs along the glacier centreline (VTG$_{CL}$) are relatively shallow, especially for warm, high-pressure conditions where a KBL begins to develop. In contrast, off-glacier VTGs become more negative due to stronger warming at CH. However, at night, the tendency towards inversions for the off-glacier data contrasts with more negative gradients for the glacier centreline (Fig. 5 and Table 3). The mean VTG for the off-glacier stations is $-0.0047\ °\mathrm{C\ m}^{-1}$ for the combined periods. The application of the off-glacier VTG (GC$_{off}$) or ELR (GC$_{ELR}$) overestimates on-glacier temperature by up to 1.5°C on average (Fig. 6a). For the warmest ambient conditions, this overestimation can be as high as 4°C for GC$_{ELR}$ (Fig. 6b) leading to an RMSE of 3.6°C compared to the measured data.
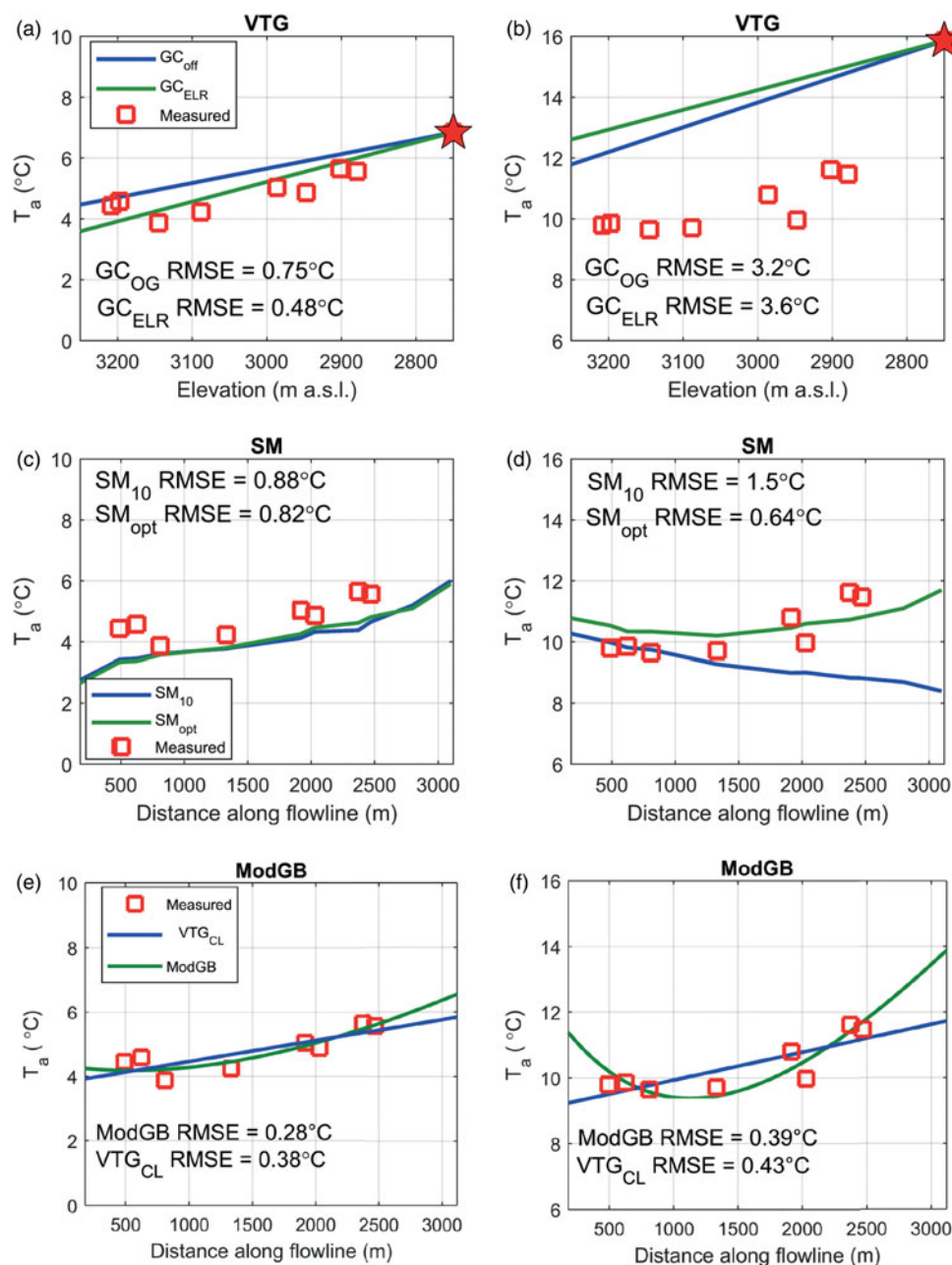

Fig. 6. Measured centreline T_a (red) and estimation of T_a for the mean of all hours (a, c, e) and the mean of the warmest T_0 bin (12–13°C, $n = 12$) (b, d, f). Panels a and b show the estimation of T_a using extrapolation with the off-glacier VTG (GC$_{off}$ – blue) and the ELR (GC$_{ELR}$ – green) from the Grand Croux station (red star). Panels c and d show estimated T_a when applying Shea and Moore with original parameters (SM$_{10}$ – blue) and recalibrated parameters (SM$_{opt}$ – green). Panels e and f show estimated T_a with the modified Greuell and Böhm model (ModGB – green), together with VTG$_{CL}$ (blue). RMSE values (°C) represent the fit of each method to the mean measured data.

Table 4. The mean 'cooling effect' (MCE) and root mean square error (RMSE) of the fit to measured data for the centreline (top half) and lateral sites (bottom half) from extrapolated temperatures using GC_{ELR}, SM_{10}, SM_{opt} and ModGB (Table 2)

Site	GC_{ELR}		SM_{10}		SM_{opt}		ModGB	
	MCE	RMSE	MCE	RMSE	MCE	RMSE	MCE	RMSE
TE1	−1.41	1.50	0.38	1.11	0.08	0.85	−1.01	1.36
TE2	−1.17	1.52	0.57	1.34	0.28	1.00	−0.72	1.41
TE3	−1.66	2.05	−0.21	1.19	−0.37	1.12	−0.96	1.50
LWS	−1.24	1.63	0.17	1.16	0.01	0.99	−0.65	1.34
TE10	−1.38	1.87	−0.34	1.27	−0.36	1.23	−0.82	1.52
UWS	−1.37	1.84	−0.57	1.37	−0.52	1.33	−1.82	2.29
TE11	−0.32	1.36	0.35	0.99	0.42	0.94	−0.86	0.97
TE13	−0.39	1.42	0.23	1.10	0.29	1.05	−1.04	1.07
Centreline	−1.12	1.65	0.07	1.19	−0.02	1.06	−0.99	1.43
TE0	−1.88	2.31	−0.15	1.24	−0.43	1.19	−1.53	1.99
TE4	−1.22	1.60	0.11	1.13	−0.01	0.99	−0.36	1.23
TE5	−1.67	2.05	−0.28	1.10	−0.43	1.07	−0.90	1.39
TE6	−1.92	2.32	−0.83	1.39	−0.83	1.38	−0.85	1.42
TE7	−0.96	1.27	−0.57	0.96	−0.47	0.94	−0.74	1.08
TE8	−1.59	1.96	−0.68	1.37	−0.65	1.32	−0.70	1.42
TE9	−1.65	2.03	−0.66	1.51	−0.65	1.43	−0.77	1.59
TE12	−0.59	1.56	−0.01	1.10	0.05	1.09	−1.23	1.06
Lateral	−1.43	1.88	−0.38	1.22	−0.42	1.17	−0.88	1.40

The MCE is calculated as measured T_a−estimated T_a. MCE and RMSE are expressed in °C. The mean of all centreline and lateral sites are also given.

The mean cooling effect (mean error) and RMSE between measured and estimated temperature at each station is given in Table 4. The mean cooling effect of all lateral stations using GC_{ELR} is −1.43°C, compared with −1.12°C for centreline stations (Table 4). Although the difference in mean cooling effect between sites for the whole period is not largely different from the measurement error of the sensors, the main differences are found in the warmest conditions (Figs 3, 4).

6.2. SM approach

The SM approach using the original (SM_{10}) and optimised (SM_{opt}) coefficients estimates mean T_a along the centreline of Tsanteleina Glacier well (Fig. 6c). For the mean of all conditions in both periods, the SM approach performs worse than using GC_{ELR} or GC_{off} (RMSE difference of 0.40 and 0.36°C for SM_{10} and SM_{opt}, respectively, compared with GC_{ELR} – Figs 6a vs c). However, for the warmest conditions at the top of the glacier flowline (T_0 = 12–13°C), the application of the SM model offers a clear improvement over GC_{ELR} (Figs 6b vs d).

However, the exponential parameterisation of k_2 from SM_{10} (blue line in Fig. 7b) does not suitably describe the cooling of T_a above the threshold for katabatic onset and thus cannot replicate the warmer T_a on the glacier tongue for the highest ambient temperatures (Fig. 6d). Although lateral observations on Tsanteleina Glacier appear to be less sensitive to ambient temperatures at greater flowline distances (small triangles in Fig. 7b), centreline k_2 parameters stabilise at ∼2000 m along the flowline and are not replicated by the exponential equation provided by SM_{10}. The k_1 parameter, however, is less variable for centreline and lateral stations compared with the k_2 parameter and similar to the values from the literature (Fig. 7a – Shea, 2010; Carturan and others, 2015). The original and optimised coefficients (Eqns (3) and (4)) are provided in Table 5.

SM_{opt} estimates T_a better at centreline locations such as TE10 than at lateral sites at similar flowline distances (e.g. TE9 – Table 4). The improvement over the use of SM_{10} is more noteworthy for centreline sites, though SM_{opt}
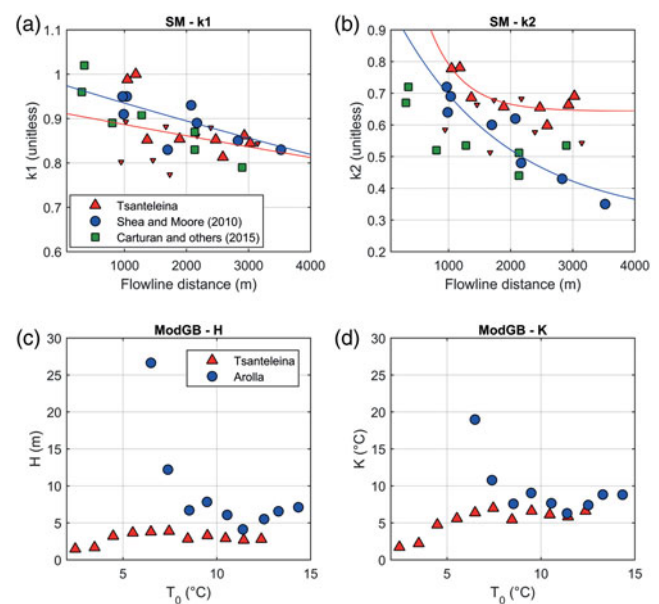
Fig. 7. Parameter values for the Tsanteleina dataset for the Shea and Moore method (SM) (a and b) and the modified Greuell and Böhm (ModGB) (c and d) compared with the parameter values from the published literature. k_1 (a) and k_2 (b) parameters are presented for Tsanteleina (red triangles – small triangles for lateral stations), the study sites of Shea and Moore (2010) (blue circles) and of Carturan and others (2015) (green squares). The parameterisations in Eqns (2) and (3) are shown for SM_{10} and SM_{opt} by the blue and red lines, respectively. ModGB parameters H (c) and K (d) are plotted as functions of T_0 for Tsanteleina Glacier (red triangles) and Arolla Glacier (blue circles). Upper panels are cropped and do not show a parameter of Shea and Moore (2010) at ∼10 000 m flowline distance.

Table 5. The parameter/coefficient set for the boundary layer models SM and ModGB as given for the current dataset and as published in the literature

Model	Parameter				
	$\beta1$	$\beta2$	$\beta3$	$\beta4$	$\beta5$
SM_{10}	0.977	$-4.4\cdot10^{-5}$	0.29	0.71	$-5.6\cdot10^{-4}$
SM_{opt}	0.913	$-2.9\cdot10^{-5}$	0.643	1	$-19.07\cdot10^{-4}$
	x_0	z_0	H (T_0 12–13)		K (T_0 12–13)
ModGB Arolla	542	3075	5.5		7.3
ModGB Tsanteleina	557	3287	2.8		6.6

Parameters for the SM model are taken from Shea (2010) and ModGB values for Arolla Glacier are taken from Ayala and others (2015). The β coefficients from Shea and Moore (2010) are originally $\beta3$–7 (for parameters k_1 and k_2).

consistently has the lowest RMSE between the measured and estimated temperatures as the k_1 and k_2 parameters are fitted to the station data for the glacier (Figs 7a, b). Lateral stations have a higher RMSE on average for SM_{opt} than centreline stations though they show the largest average improvement in RMSE compared to GC_{ELR} (Table 4).

6.3. Application of ModGB

Under warm ambient temperatures (temperature at $T_0 \geq 6°$ C), ModGB is able to replicate the initial down-glacier cooling effect and warming on the glacier tongue (Figs 6e, f). Fitted parameters H and K are ~2–3 m and 6–7°C, respectively, for $T_0 \geq 6°C$, smaller and more stable values than those found by Ayala and others (2015) for Arolla Glacier (Table 5, Figs 7c, d).

For comparison with ModGB, all methods of T_a distribution are binned into T_0 intervals to assess their performance at replicating on-glacier temperature (Fig. 8). The ModGB approach better fits to the mean measured centreline data than the other temperature distribution methods (based on RMSE) for all T_0 bins. Compared with GC_{ELR}, the SM approaches and ModGB are both superior because the cooling effect of the glacier surface is accounted for, even when including lateral T_a variability (crosses in Fig. 8a). For cooler ambient conditions (e.g. $T_0 = 2$–5°C), the application of GC_{ELR} is more appropriate for representing on-glacier temperatures, but is still out-performed by the on-glacier T_a distribution models. Even compared with VTG_{CL}, ModGB has a lower RMSE for the warmest ambient conditions (Fig. 8b). This is, however, the result of inappropriate fitting of the ModGB equation when the air temperature is more linear with elevation (Fig. 6e). In a time-series application, ModGB reduces error compared to GC_{ELR}, but is out-performed in modelling hourly T_a by the SM approaches (Table 4). The suitability of extracted parameters is an important consideration for the ModGB approach which is addressed in the Discussion section.

Model errors are greater when ModGB is assessed against all T_a data (including non-centreline) for all ambient temperature ranges (RMSE of 1.1°C for $T_0 = 12$–13°C, red crosses in Fig. 8). However, ModGB is not, by definition, designed to account for marginal temperature variability. Furthermore, the SM_{opt} method (Fig. 8a) or VTG_{CL} (Fig. 8b) also lead to a high RMSE of 1.17 and 0.99°C, respectively, for $T_0 = 12$–13°C and much of the variability in lateral T_a under warm ambient conditions is also poorly estimated.

7. RESULTS: MELT MODELLING

7.1. Validation of melt models

'Reference model' melt values are provided by running the energy-balance model using meteorological inputs as described in the Methods section and measured on-glacier T_a at each T-logger/AWS site (Fig. 9). There is a tendency towards model underestimation in Jul–Aug and overestimation in Aug–Sep, but RMSEs of 0.0030 m w.e. d^{-1} in Jul–Aug and 0.0034 m w.e. d^{-1} in Aug–Sep are acceptable given potential error sources in both model and data (error bars in Fig. 9). Notably, reference model melt and stake
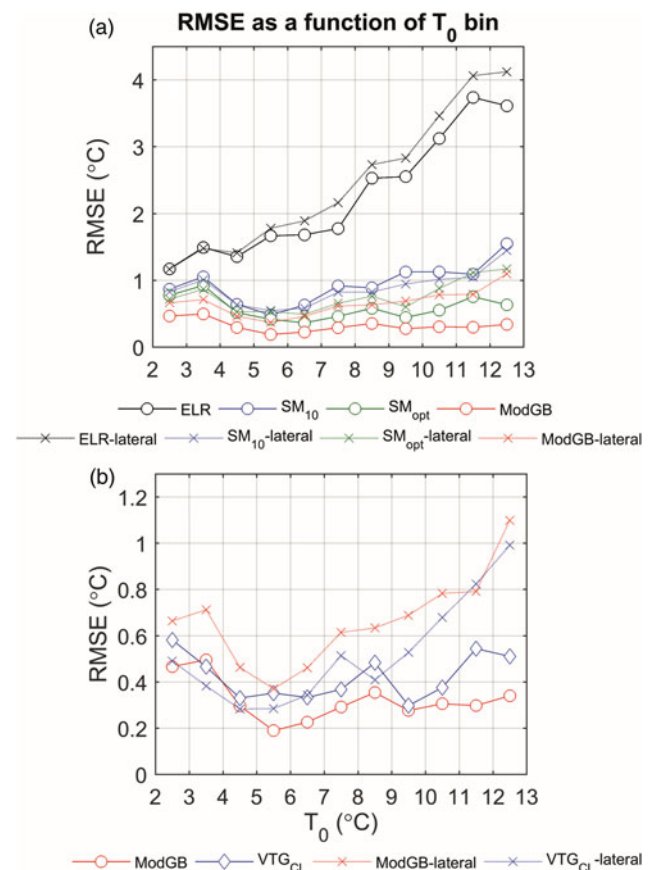

Fig. 8. Calculated RMSE (°C) of measured T_a and estimated T_a using GC_{ELR}, SM_{10}, SM_{opt} and ModGB for T_0 bins (panel a). Panel b shows the same ModGB performance relative to the RMSE of VTG_{CL} as a function of T_0 bins. RMSE calculated using the measured mean data for centreline stations and all stations ('lateral') for each T_0 bin.
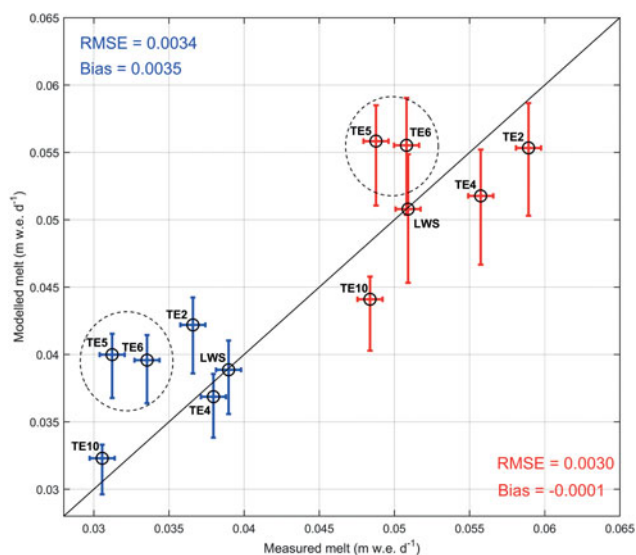
Fig. 9. Reference measured vs modelled average daily ablation (m w.e. d^{-1}) for all stake data in Jul–Aug (red) and Aug–Sep (blue) with the RMSE for the fit in each period. An error range of 5 cm (Reid and others, 2012) for each period is shown by the horizontal error bars (averaged over the number of days). Vertical error bars indicate the uncertainty associated with a uniform air temperature perturbation of ±0.35°C. The dashed circles indicate sites of consistent model overestimation associated with calm wind flow (see text).

ablation agree very well at LWS in both periods, suggesting extrapolation of meteorological input variables and glacier parameters accounts for at least some of the scatter between model and data. Distribution of wind is a possible cause of strong melt overestimation at TE5 and TE6 in both periods (circled) which are considered to be topographically sheltered areas of the glacier (see Discussion section). Measured daily average melt range from 0.048 to 0.059 m w.e. d^{-1} for Jul–Aug and 0.030 to 0.038 m w.e. d^{-1} for Aug–Sep.

7.2. Distributed temperature and modelled melt rates

Figure 10 shows the daily mean melt rates for model runs with the distribution of T_a using VTGs, ModGB or SM approaches. These results (solid coloured circles) are compared with measured stake data and reference model runs as in Figure 9 (hollow black circles and error bars). The RMSE and bias of all model runs are shown in Table 6.

VTG$_{CL}$ provides a good fit to the measured melt rates at stake locations (RMSE = 0.0032 m w.e. d^{-1} in Jul–Aug) as it represents the on-glacier recorded T_a at LWS and a VTG calculated from several on-glacier T-loggers (Fig. 5 upper panel, Fig. 10a). T_a extrapolation from off-glacier sites using VTGs results in model overestimation (a positive bias). For example, melt at LWS is overestimated by ~0.006–0.010 m w.e. d^{-1} using all three VTG methods during Jul–Aug (Table 6). This overestimation of the melt is shown for GC$_{ELR}$ in Figure 10b.

SM$_{10}$ is found to underestimate melt rates at many sites compared to the reference run (negative bias), particularly at lower elevations/greater flowline distances (Fig. 10e). The application of SM$_{opt}$ provides improved melt model performance compared to SM$_{10}$, though still underestimates the reference model melt rate at some stations (Fig. 10f). For

lateral sites TE5 and TE6, SM$_{opt}$ performs similarly to the reference. Performance of SM$_{10}$ and SM$_{opt}$ is very similar for the cooler Aug–Sep period.

The application of ModGB for $T_0 \geq 6°C$ (the convergence of H/K in the literature – Ayala and others, 2015, 2017) resulted in an RMSE reduction of 0.0023 m w.e. d^{-1} compared with an off-glacier VTG distribution (Fig. 10d), in spite of only ~35% of the total time steps at T_0 being $\geq 6°$C, and T_a was otherwise distributed using a GC$_{ELR}$ approach. As H and K parameters are stable for all T_0 ranges on Tsanteleina Glacier (Figs 7c, d), ModGB was also run for $T_0 \geq 2°C$. However, as this method is designed for warm ambient temperatures, reducing this threshold implies a too greater warming effect on the glacier tongue for cooler ambient temperatures and melt rates are overestimated at TE2 (Fig. 10c). Applying ModGB for $T_0 \geq 2°C$ nevertheless improved estimates of melt compared to GC$_{ELR}$.

The use of the SM and ModGB temperature distribution methods improves modelled melt rates by an RMSE of between 0.0020 and 0.0024 m w.e. d^{-1} (28–36% RMSE reduction) compared to GC$_{ELR}$, though only SM$_{opt}$ is statistically similar to the on-glacier VTG$_{CL}$ distribution when compared to the reference model using a Wilcoxon ranked-sum test (Table 6). In the context of model errors, both ModGB (for $T_0 \geq 6°C$) and the SM approaches are within the maximum uncertainty of T_a records assuming a uniform ±0.35°C air temperature perturbation.

8. DISCUSSION

8.1. Temperature distribution and VTGs

The weak dependence of centreline temperature on elevation under warm ambient conditions recorded at Tsanteleina Glacier concurs with the majority of previous findings regarding katabatic effects on T_a distribution (e.g. Greuell and Böhm, 1998; Shea and Moore, 2010; Petersen and others, 2013; Ayala and others, 2015). However, on-glacier VTGs were on average more negative than found in previous studies (e.g. Strasser and others, 2004; Carenzo, 2012; Marshall, 2014). Tsanteleina Glacier likely has a thin boundary layer due to its small size, and a katabatic flow influence on centreline T_a distribution only dominates for high ambient temperatures (Fig. 6f, Table 3). Carturan and others (2015) also derived gradients that are steeper than the ELR over a small glacier with a similar northeast orientation (La Mare Glacier) to Tsanteleina Glacier. They attributed this in part to station positioning and the presence of steeper slopes above a lower station, which resulted in the dominance of adiabatic heating under compression (Greuell and others, 1997; Greuell and Böhm, 1998, Strasser and others, 2004). On Tsanteleina Glacier, the strong negative VTGs derived by regression of multiple stations with elevation (Fig. 3) would not be strongly influenced by such site-specific factors, however. Although VTG$_{CL}$ poorly accounts for the structure of on-glacier T_a variability under the warmest conditions, it still performs well at modelling daily average melt rates relative to the reference model (Fig. 10a). However, as both on-glacier data and locally-derived VTG would typically be unavailable for regional and larger scale studies over unmonitored glaciers, it is important that the temperature distribution models using off-glacier T_a be applied with generalisable parameters and thresholds.
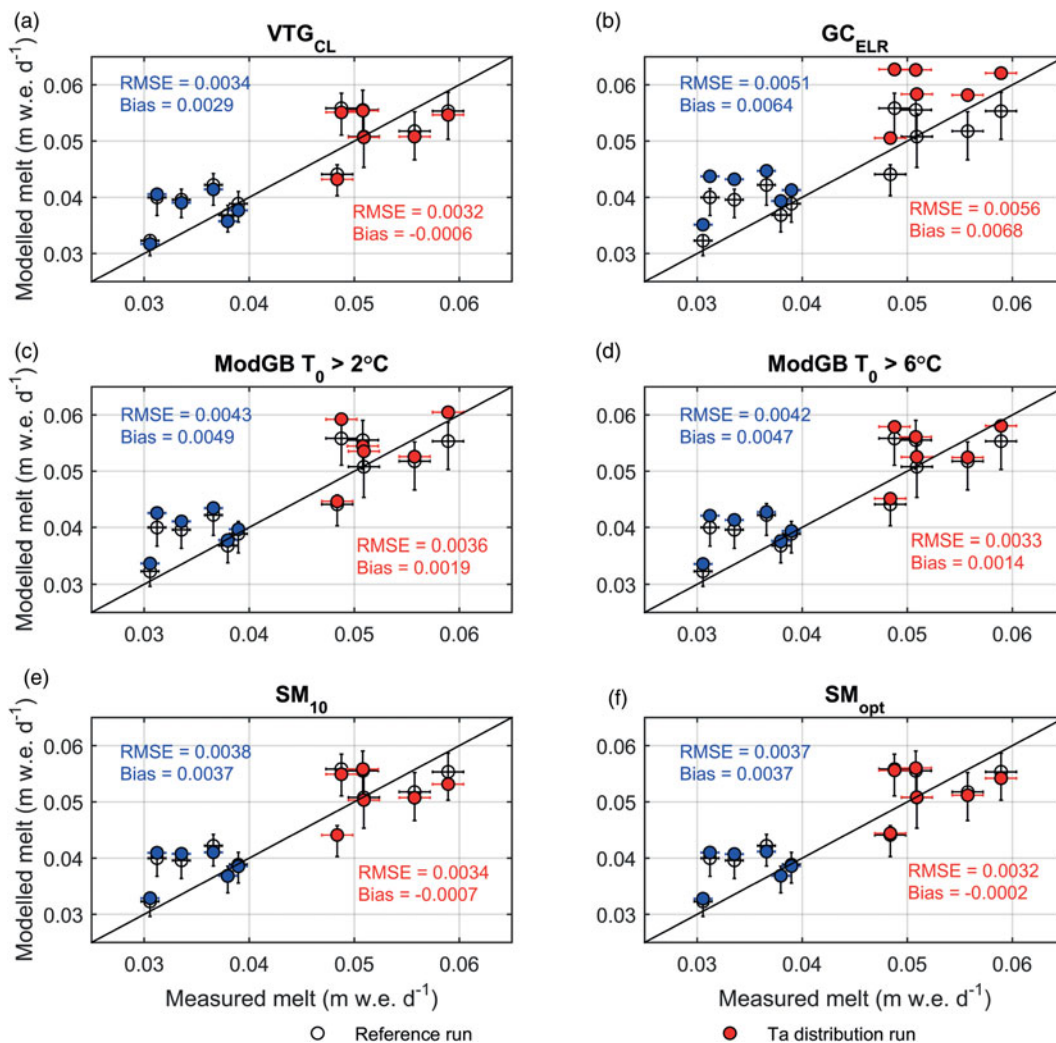
Fig. 10. Measured and modelled daily average melt (m w.e. d^{-1}) at stake sites using different T_a distribution methods (see Table 2). Data are shown for selected centreline and lateral sites with observations in both Jul–Aug (red) and Aug–Sep (blue) (see Fig. 9). Horizontal error bars indicate a 5 cm error for measured ablation and vertical error bars indicate the uncertainty associated with a uniform air temperature perturbation of ±0.35°C in the reference model. RMSE and mean bias values are reported in m w.e. d^{-1} for each model run/period. Panel c shows the performance of ModGB if applied to all T_0 temperatures ≥2°C. Metrics of all model runs are shown in Table 6.

For warm ambient conditions (where top-of-flowline temperatures exceed 6°C), the application of an off-glacier VTG was found to be unsuitable for estimating on-glacier temperature. This is because off-glacier stations are (a) outside the influence of the glacier boundary layer and (b) affected by local topographic influences on temperature, e.g. shading, cold air drainage. Several previous studies have found similar issues with off-glacier temperature extrapolation

Table 6. RMSE and mean bias of melt model results for the different temperature distribution methods (reported in m w.e. d^{-1})

Model	Jul–Aug			Aug–Sep		
	RMSE	Bias	p-value	RMSE	Bias	p-value
Reference	0.0030	−0.0001	–	0.0034	0.0035	–
VTG$_{CL}$	0.0032	−0.0006	–	0.0034	0.0029	–
GC$_{ELR}$	0.0056	0.0068	0.001	0.0051	0.0064	0.001
GC$_{off}$	0.0056	0.0069	0.001	0.0046	0.0054	0.001
CH$_{ELR}$	0.0057	0.0070	0.001	0.0038	0.0034	0.001
ModGB ($T_0 ≥ 2$)	0.0036	0.0019	0.002	0.0043	0.0049	0.001
ModGB ($T_0 ≥ 6$)	0.0033	0.0014	0.003	0.0042	0.0047	0.001
SM$_{10}$	0.0034	−0.0007	0.017	0.0038	0.0037	0.001
SM$_{opt}$	0.0032	−0.0002	**0.612**	0.0037	0.0037	0.002

P-values indicate the results of a Wilcoxon rank-sum test of the statistical differences in the median RMSE between the reference model results at all stakes and different T_a distribution methods compared to the use of an on-glacier VTG (VTG$_{CL}$). The reported *p*-values indicate the statistically significant differences compared to VTG$_{CL}$ at the 95% level for Jul–Aug and Aug–Sep. Where $p > 0.05$, the method does not perform significantly different to the use of on-glacier data and a local VTG (these instances are shown in bold).

(Shea and Moore, 2010; Carturan and others, 2015). Hence, alternative parameterisations or corrections for T_a distribution are required to distribute on-glacier temperatures. It is difficult to determine what off-glacier sites are truly 'representative' and suitable for extrapolation of temperature to the elevation of the glacier. Exploratory analyses revealed that deriving temperature gradients between a series of local stations at higher elevations than CH in the neighbouring valleys produced similarly shallow VTGs, mostly likely due to topographically induced air circulation patterns and their effects on valley sites. Therefore, the initial temperatures (T_0 and T_{amb}) of the boundary layer temperature estimation methods were extrapolated from GC using the ELR.

8.2. Application of on-glacier temperature distribution models

In this study, T^* from the SM method was parameterised as a function of the flowline distance (Eqn (2)) following Carturan and others (2015) because the original method (as a linear function of elevation (Shea and Moore, 2010)) resulted in low T^* values across the glacier (3.1–3.8°C). In the original SM_{10} model, values of the k_2 parameter decrease continuously with increasing flowline distance, whereas k_2 parameter values derived from the Tsanteleina data are higher for equivalent flowline distances and level off beyond 2000 m (Fig. 7b). Such marked spatial variation in the k_2 parameter means that the SM approach requires further evaluation and development to account for local effects on KBL development before it can be applied generally. The levelling-off of k_2 parameter values at short flowline distances in both this study and Carturan and others (2015) (green triangles in Fig. 7b) suggests that, for small glaciers, the continued down-glacier cooling effect may be generally absent (Fig. 6d). This is particularly the case for the occurrence of warmer temperatures on the tongue of Tsanteleina Glacier which are better modelled by the ModGB approach. It is perhaps unlikely that the SM_{opt} parameterisation (red line in Fig. 7b) will be transferable to other glacier sites, though it emphasises the requirement for more distributed datasets to calibrate a globally applicable parameter set which may act as a function of glacier size. Over larger flowline distances, it has been suggested that the development of the KBL is sufficient to minimise the influence of free-atmospheric temperatures and that the coolest on-glacier temperatures are experienced at the glacier terminus (Greuell and Böhm, 1998; Shea and Moore, 2010). In this instance, SM_{opt} still underestimates melt at some sites (Fig. 10), though provides an improved fit (RMSE) to the data compared with SM_{10}.

ModGB had the lowest RMSE of all the temperature distribution methods (Fig. 8) as well as a linear on-glacier VTG (Figs 6e, f) when estimating mean T_a for most T_0 bins. The parameters H and K were smaller than those obtained for Arolla Glacier (Figs 7c, d), likely due to the glacier's size which has insufficient fetch to create a strong KBL and lacks length to sustain it. Of local significance to Tsanteleina Glacier is the fact that the dominant synoptic wind direction from the west is aligned with the down-glacier flow at LWS. Identifying a clear switch between katabatic conditions and erosion by synoptic-scale events is therefore difficult. Nevertheless, during periods of strong, synoptically driven winds, temperature gradients were highly linear and negative (Table 3) and lateral differences

reduced because of the lack of identified glacier 'cold spots' (Fig. 4).

In general, ModGB appears to be a useful tool for explaining along-flowline T_a variability that has a physical basis. The development of this thermodynamic approach has led to improvements in RMSE compared to off-glacier or on-glacier VTGs (Greuell and Böhm, 1998; Petersen and others, 2013; Ayala and others, 2015; Carturan and others, 2015). Nevertheless, as a practical solution to modelling glacier melt rates; there remains a continued uncertainty about the threshold conditions for the implementation of ModGB that needs to be further explored. For example, as the H and K parameters are calibrated for warm ambient temperatures (Figs 7c, d), they are unsuitable for cool conditions (suggestions from Arolla Glacier (Ayala and others, 2015) and Juncal Norte Glacier, Chile (Ayala and others, 2017)), and therefore a threshold for the application of ModGB is required. In this respect, although the ModGB performs better than the SM approach at explaining mean conditions as a function of T_0 temperatures when it is fitted to the data (Figs 6, 8), it is outperformed by the SM approach in estimating individual hourly temperatures (Table 4) and melt rates (Fig. 10d) at individual stations, particularly at lateral locations. This is largely the result of the poor estimation of T_a for hours below the temperature threshold, which is still estimated by GC_{ELR}. Applying ModGB above a lower threshold (2°C) inadequately represented hourly temperatures and melt rates on the lower glacier (Fig. 10c) and demonstrates that appropriate thresholds are important. Although both ModGB (for $T_0 \geq 6$°C) and SM methods modelled daily average melt within the maximum uncertainty of the temperature sensors (Fig. 10), they require further development before large-scale deployment in regional glacier studies.

A constraint for the distribution of T_a using SM and ModGB is that they are designed to only account for T_a changes along a glacier centreline where katabatic conditions are theoretically strongest. These methods likely cannot represent mean measured data at lateral station locations due to the fact that these sites can be affected by advection of warm air from surrounding topography (e.g. TE4 – Hannah and others, 2000), localised cooling (Fig. 4) or that sensible and latent heat exchanges can be reduced near to glacier margins outside the influence of the KBL (Shea and Moore, 2010). Estimation of temperatures using the SM approach is worse on average for lateral locations compared with centreline stations (Table 4), though the performance of most approaches is not clearly superior at centreline locations in the results of an energy-balance model (Fig. 10).

The selection of the most appropriate model for estimating T_a over mountain glaciers could be considered with respect to the number of parameters and the amount of fitting to large datasets it requires. The SM approach has eight unknowns ($\beta1$–5, $C1$–2 and the value of the VTG used to extrapolate initial temperature) and ModGB has four (H, K, x_0 and the off-glacier VTG). Although direct comparison of method performance based on parameter quantity is not feasible with such different approaches, the lower RMSE of the SM methodology for estimating hourly temperatures could be argued to be related to its reliance on double the number of parameters that ModGB requires. Nevertheless, as is evident from the inappropriate fitting of ModGB to data for cooler conditions (Figs 6e, 8), its application necessitates a further threshold value which is also sensitive to the location and elevation of the point where air enters the KBL

(x_0). Further still, it is found that the stability of extracted parameters H and K may vary between different sites (Figs 7c, d), and so the threshold conditions for application of ModGB may be more necessary in certain cases than others. Crucially, the exact processes causing warmer air temperatures on glacier tongues is still uncertain (e.g. Sauter and Galos, 2016), and so selecting the optimum method for distributing air temperatures in long-term glacier melt models remains unclear. The ModGB approach has clear advantages for calculation of air temperature for the warmest conditions on Tsanteleina Glacier, but when utilised for calculation of melt rates, its performance decreases because it relies on the accuracy of an off-glacier gradient below the threshold temperature. Because of its physical basis, the derivation of parameters (such as the height of the boundary layer, H) may be afforded by other datasets such as tower measurements or radiosondes (Greuell and Böhm, 1998). Alternatively, the parameterisation suggested by Shea and Moore (2010), though potentially more generally applicable, is only statistical in nature and currently does not account for the warming on glacier tongues.

A final consideration is the sensitivity of these methods to different temperature extrapolation from the off-glacier site GC. As the local VTG is a generally unknown value (as stated above), the current boundary layer models have been forced with high elevation T_a and the ELR (-0.0065 °C m^{-1}). However, high variability in locally derived off-glacier VTGs (Fig. 5) will introduce uncertainty and this needs to be further addressed as such boundary layer models become more generalisable and require initial temperature forcing data.

8.3. Glacier 'cold spots' and distributed wind speed

Sites TE0, TE3, TE6 and TE12 exhibited consistently colder T_a relative to sites at similar elevations or flowline distances on the glacier for warm ambient conditions (Fig. 3). These 'cold spots' at TE6 and TE12 are hypothesised to be due to topographic depressions in the glacier surface which promote the entrapment of radiatively cooled stagnant air under calm, high-pressure conditions (Fig. 4). Topographic depressions coincident with the sites of TE6 and TE12 can be inferred from analysis using GIS hydrology 'sink' tools (results not shown) but the available ASTER DEM is of too coarse resolution (30 m) to provide a robust test of this hypothesis. Differences in modelled global radiation at lateral and centreline sites were small (<10 W m^{-2} on average between TE6 and LWS) and the intercomparison tests (see Supplementary Material) found that the naturally ventilated T_a measurements were not noticeably affected by moderately low wind speed conditions in the presence of insolation, lending support to the legitimacy of these observations.

Less clear is the cause of low-temperature anomalies at centreline site TE3, which occurred under both high and low wind speeds (Fig. 4). Temperatures along this part of the flowline are, however, consistent with findings of Foessel (1974) and Munro (2006) who explain 'cold spots' from the convergence of tributary air flows on Peyto Glacier, Canada. Convergence of air at LWS and TE3 from the southern limb of Tsanteleina Glacier (Fig. 1) could increase the boundary layer thickness and limit the entrainment of warmer free air (Munro, 2006), thus accounting for cooling at TE3 (also during windier conditions).

Furthermore, the pattern of anomalies of T_a at TE0 was similar to that found at TE6 (Fig. 4), though differences in modelled radiation were very small. TE0 was considered as a lateral site for this investigation, though its distance from TE1 (with warmer observations of T_a) is only ~100 m. This raises questions about the processes influencing near-surface air temperatures at different locations on the glacier tongue and how well they are represented by either VTGs or alternative models tested in this study.

Overestimation of wind speed at TE6 and TE5 is a possible reason for overestimation of melt rate when using the locally measured T_a (Fig. 9). Artificially halving the wind speed in the melt model at these locations results in a close match to measured melt rates. Following the method proposed by Winstral and others (2002), the exposure of different model gridcells across the glacier was determined using wind direction measured at both AWS sites and the elevation information from the DEM (results not shown). While this is a crude approach given the DEM resolution, both TE6 and TE5 (as well as TE12 – Fig. 4) are suggested to be sheltered from the dominant westerly wind direction by the surrounding topography and lower wind speeds at these sites are potentially likely. Modelling distributed wind fields across glaciers remain problematic and an area for future research beyond the scope of this paper.

9. CONCLUSIONS

This study has analysed a network of centreline and lateral air temperature observations over an alpine glacier during the 2015 summer ablation season. Two recently published methods from the literature that attempt to reproduce the cooling of air temperature over a melting glacier were tested and applied to an energy-balance model. The key findings of this work are:

(1) When top-of-flowline ambient air temperatures are low (<6°C), VTGs (e.g. the linear variation of temperature with elevation) can reproduce temperature variability. However, when ambient temperatures are high (>6°C), on-glacier air temperatures are only weakly dependent on elevation and a VTG is inappropriate for its estimation, particularly when extrapolated from an off-glacier location that does not account for the glacier cooling effect.

(2) The two alternative methods proposed in the literature by Shea and Moore (2010) and Ayala and others (2015) improve estimates of on-glacier air temperature for warm ambient conditions compared with the use of off-glacier temperature gradients, because they account for the glacier cooling effect (RMSE reduction of up to 2.9°C). However, recalibration of their parameters is still necessary to improve simulation of surface melt in energy-balance models. The use of the above temperature estimation methods improves modelled melt rates with an RMSE reduction of 28–36% compared with the use of non-corrected off-glacier lapse rate.

(3) Both methods, while being important advancements, have the potential for improvements. The ModGB approach by Ayala and others (2015) is the best method for calculations of air temperature for the warmest conditions on Tsanteleina Glacier, but when utilised for calculation of melt rates, its performance decreases because it relies on the accuracy of an

off-glacier gradient below the threshold temperature. Alternatively, the parameterisation suggested by Shea and Moore (2010) does not account for the warming on glacier tongues, which has been demonstrated in recent publications.

(4) Lateral 'cold spots' were found to be >2°C cooler than the equivalent centreline elevation under moderately low wind speed, warm and high-pressure conditions. These observations cannot be replicated by either a VTG or the alternative methods (and might be even more important for modelling melt on larger glaciers). The causes of high and low temperatures relative to the centreline require further investigation for its implications to long-term glacier mass balance, particularly in relation to distributed values of wind speed.

To the authors' knowledge, this is the first study that has objectively assessed the performance of these two newly developed temperature distribution models compared to an on-glacier distribution of centreline and lateral temperature records. Our results provide evidence that accounting for the cooling effect of the glacier boundary layer is most crucial to short-term energy-balance modelling, though local influences from 'cold spots', distributed wind speeds and warm temperatures on the glacier tongue may also need consideration for longer term glacier modelling. Based on these findings, we suggest that further work in this field attempt to establish more low-cost networks of on-glacier temperature records to build towards a globally applicable parameterisation for the glacier cooling effect over a range of glacier sizes.

SUPPLEMENTARY MATERIAL

The supplementary material for this article can be found at https://doi.org/10.1017/jog.2017.65.

ACKNOWLEDGEMENTS

REFERENCES

Anslow FS, Hostetler S, Bidlake WR and Clark PU (2008) Distributed energy balance modeling of South Cascade Glacier, Washington and assessment of model uncertainty. *J. Geophys. Res.*, **113**(F2), F02019 (doi: 10.1029/2007JF000850)

Arnold NS, Rees WG, Hodson AJ and Kohler J (2006) Topographic controls on the surface energy balance of a high Arctic valley glacier. *J. Geophys. Res.*, **111**(F2), F02011 (doi: 101029/2005JF000426)

Ayala A, Pellicciotti F and Shea JM (2015) Modeling 2 m air temperatures over mountain glaciers: exploring the influence of katabatic cooling and external warming. *J. Geophys. Res. Atmos.*, **120**, 1–19 (doi: 10.1002/2015JD023137)

Ayala A, Pellicciotti F, Peleg N and Burlando P (2017) Distributed modelling of the summer energy balance of Juncal Norte Glacier, Chile: estimating melt and surface sublimation rates at high- elevation unmonitored sites. *J. Glaciol.*, Accepted – April, 2017

Brock BW and Arnold NS (2000), A spreadsheet-based (Microsoft Excel) point surface energy balance model for glacier and snow melt studies. *Earth Surf. Process. Landforms*, **25** 649–658 (doi: 10.1002/1096-9837(200006)25:6<649: AID-ESP97>3.0. CO;2-U)

Brock BW, Willis IC and Sharp MJ (2006) Measurement and parameterization of aerodynamic roughness length variations at Haut Glacier d'Arolla, Switzerland. *J. Glaciol.*, **52**(177), 281–F02297

Carenzo M (2012) Distributed modelling of changes in glacier mass balance and runoff. (PhD thesis, ETH Zürich)

Carturan L, Cazorzi F, De Blasi F and Dalla Fontana G (2015) Air temperature variability over three glaciers in the Ortles–Cevedale (Italian Alps): effects of glacier fragmentation, comparison of calculation methods, and impacts on mass balance modeling. *Cryosphere*, **9**(3), 1129–1146 (doi: 10.5194/tc-9-1129-2015)

Engelhardt M, Schuler TV and Andreassen LM (2013) Glacier mass balance of Norway 1961–2010 calculated by a temperature-index model. *Ann. Glaciol.*, **54**(63), 32–40 (doi: 10.3189/2013AoG63A245)

Foessel DG (1974) An analysis of the temperature distribution over the Peyto Glacier, Alberta. (M.Sc. thesis, University of Guelph)

Fyffe CL and 6 others (2014) A distributed energy-balance melt model of an alpine debris-covered glacier. *J. Glaciol.*, **60**(221), 587–602 (doi: 10.3189/2014JoG13J148)

Gabbi J, Carenzo M, Pellicciotti F, Bauder A and Funk M (2014) A comparison of empirical and physically based glacier surface melt models for long-term simulations of glacier response. *J. Glaciol.*, **60**(224), 1140–1154 (doi: 10.3189/2014JoG14J011)

Georges C and Kaser G (2002) Ventilated and unventilated air temperature measurements for glacier-climate studies on a tropical high mountain site. *J. Geophys. Res.*, **107**, 4775 (doi: 10.1029/2002JD002503)

Greuell W and Böhm R (1998) 2 m temperatures along melting midlatitude glaciers, and implications for the sensitivity of the mass balance to variations in temperature. *J. Glaciol.*, **44**(146), 9–20

Greuell W, Knap WH and Smeets PC (1997) Elevational changes in meteorological variables along a midlatitude glacier during summer. *J. Geophys. Res.*, **102**(D22), 25941 (doi: 10.1029/97JD02083)

Hannah DM, Gurnell AM and McGregor GR (2000) Spatio-temporal variation in microclimate, the surface energy balance and ablation over a cirque glacier. *Int. J. Climatol.*, **20**(7), 733–758 (doi: 10.1002/1097-0088(20000615)20:7<733::AID-JOC490>3.0. CO;2-F)

Hock R (1999) A distributed temperature-index ice- and snowmelt model including potential direct solar radiation. *J. Glaciol.*, **45**(149), 101–111

Hock R, de Woul M, Radić V and Dyurgerov M (2009) Mountain glaciers and ice caps around Antarctica make a large sea level rise contribution. *Geophys. Res. Lett.*, **36**(7), L07501 (doi: 10.1029/2008GL037020)

Jóhannesson T, Sigurðsson O, Laumann T and Kennett M (1995) Degree-day glacier mass-balance modelling with applications to glaciers in Iceland, Norway and Greenland. *J. Glaciol.*, **41**(138), 345–358

Juszak I and Pellicciotti F (2013) A comparison of parameterizations of incoming longwave radiation over melting glaciers: model robustness and seasonal variability. *J. Geophys. Res. Atmos.*, **118**(8), 3066–3084 (doi: 10.1002/jgrd.50277)

Konya K, Hock R and Naruse R (2007) Temperature lapse rates and surface energy balance at Storglaciären, northern Sweden. *Glacier Mass Balance Meltwater Discharge*, (selected papers from sessions at the IAHS Assembly in Foz do Iguaçu, Brazil, 2005). IAHS Publ. 318, 186–194

MacDougall AH and Flowers GE (2011) Spatial and temporal transferability of a distributed energy-balance glacier melt model. *J. Clim.*, **24**(5), 1480–1498 (doi: 10.1175/2010JCLI3821.1)

MacDougall AH, Wheler B and Flowers GE (2011) A preliminary assessment of glacier melt-model parameter sensitivity and transferability in a dry subarctic environment. *Cryosphere*, **5**(4), 1011–1028 (doi: 10.5194/tc-5-1011-2011)

Marshall SJ (2014) Meltwater run-off from Haig Glacier, Canadian Rocky Mountains, 2001–2013. *Hydrol. Earth Syst. Sci.*, **18**(12), 5181–5200 (doi: 10.5194/hess-18-5181-2014)

Marshall SJ, Sharp MJ, Burgess DO and Anslow FS (2007) Near-surface-temperature lapse rates on the Prince of Wales Icefield, Ellesmere Island, Canada: implications for regional downscaling of temperature. *Int. J. Climatol.*, **27**, 385–398 (doi: 101002/joc)

Munro DS (1989) Surface roughness and bulk heat transfer on a glacier: comparison with eddy correlation. *J. Glaciol.*, **35**(121), 343–348

Munro DS (2006) Linking the weather to glacier hydrology and mass balance at Peyto glacier. *Peyto Glacier One Century Sci.*, National Hydrology Research Institute Science Report 8, 135–178

Nolin AW, Phillippe J, Jefferson A and Lewis SL (2010) Present-day and future contributions of glacier runoff to summertime flows in a Pacific Northwest watershed: implications for water resources. *Water Resour. Res.*, **46**(12), n/a–n/a (doi: 10.1029/2009WR008968)

Oerlemans J (2001) *Glaciers and climate change*. AA Balkema, Lisse

Ohata T (1992) An evaluation of scale-dependent effects of atmosphere-glacier interactions on heat supply to glaciers. *Ann. Glaciol.*, **16**, 115–122

Ohmura A (2001) Physical basis for the temperature-based melt-index method. *J. Appl. Meteorol.*, **40**(4), 753–761

Pellicciotti F and 7 others (2008) A study of the energy balance and melt regime on Juncal Norte Glacier, semi-arid Andes of central Chile, using melt models of different complexity. *Hydrol. Process.*, **22**, 3980–3997 (doi: 10.1002/hyp)

Pellicciotti F, Ragettli S, Carenzo M and McPhee J (2014) Changes of glaciers in the Andes of Chile and priorities for future work. *Sci. Total Environ.*, **493C**(2014), 1197–1210 (doi: 10.1016/j.scitotenv.2013.10.055)

Petersen L and Pellicciotti F (2011) Spatial and temporal variability of air temperature on a melting glacier: atmospheric controls, extrapolation methods and their effect on melt modeling, Juncal Norte Glacier, Chile. *J. Geophys. Res.*, **116**(D23), D23109 (doi: 10.1029/2011JD015842)

Petersen L, Pellicciotti F, Juszak I, Carenzo M and Brock BW (2013) Suitability of a constant air temperature lapse rate over an alpine glacier: testing the Greuell and Böhm model as an alternative. *Ann. Glaciol.*, **54**(63), 120–130 (doi: 10.3189/2013AoG63A477)

Ragettli S and Pellicciotti F (2012) Calibration of a physically based, spatially distributed hydrological model in a glacierized basin: on the use of knowledge from glaciometeorological processes to constrain model parameters. *Water Resour. Res.*, **48**(3) (doi: 10.1029/2011WR010559)

Reda I and Andreas A (2008) Solar Position Algorithm for Solar Radiation Applications, National Renewable Energy Laboratory. *Technical Report NREL/TP-560-34302*. US Department of Energy, Oak Ridge

Reid TD, Carenzo M, Pellicciotti F and Brock BW (2012) Including debris cover effects in a distributed model of glacier ablation. *J. Geophys. Res. Atmos.*, **117**(D18) (doi: 10.1029/2012JD017795)

Reijmer CH and Hock R (2008) Internal accumulation on Storglaciaren, Sweden, in a multi-layer snow model coupled to a distributed energy- and mass-balance model. *J. Glaciol.*, **54**(184), 61–72

Sauter T and Galos SP (2016) Effects of local advection on the spatial sensible heat flux variation on a mountain glacier. *Cryosphere*, **10**, 1–30 (doi: 10.5194/tc-2016-139).

Shaw TE and 5 others (2016) Air temperature distribution and energy-balance modelling of a debris-covered glacier. *J. Glaciol.*, **62** (doi: 10.1017//jog.2016.31)

Shea J (2010) Regional-scale distributed modelling of glacier meteorology and melt, southern Coast Mountains, Canada. PhD thesis, University of British Columbia

Shea JM and Moore RD (2010) Prediction of spatially distributed regional-scale fields of air temperature and vapor pressure over mountain glaciers. *J. Geophys. Res.*, **115**(D23), D23107 (doi: 10.1029/2010JD014351)

Steiner JF and Pellicciotti F (2016) Variability of air temperature over a debris-covered glacier in the Nepalese Himalaya. *Ann. Glaciol.*, **57**(71), 295–307 (doi: 10.3189/2016AoG71A066)

Strasser U and 5 others (2004) Spatial and temporal variability of meteorological variables at Haut Glacier d'Arolla (Switzerland) during the ablation season 2001: measurements and simulations. *J. Geophys. Res.*, **109**, D03103 (doi: 10.1029/2003JD003973)

Tachikawa T, Hato M, Kaku M and Iwasaki A (2011) *The characteristics of ASTER GDEM version 2*. Geoscience and Remote Sensing Symposium (IGARSS), IEEE International, British Columbia, Canada, 24-29 July 2011

van den Broeke MR (1997) Momentum, heat, and moisture budgets of the katabatic wind layer over a midlatitude glacier in summer. *J. Appl. Meteorol.*, **36**(1987), 763–774

van de Wal RSW, Oerlemans J and van der Hage JC (1992) A study of ablation variations on the tongue of Hintereisferner, Austrian Alps. *J. Glaciol.*, **38**(130), 319–324

Winstral A, Elder K and Davis RE (2002) Spatial snow modeling of wind-redistributed snow using terrain-based parameters. *J. Hydrometeorol.*, **3**(5), 524–538 (doi: 10.1175/1525-7541(2002)003<0524:SSMOWR>2.0.CO;2)